Journal of Thermal Analysis and Calorimetry, Vol. 57 (1999) 831-838

IMPROVEMENT OF ELECTRICAL CONDUCTIVITY IN FLUORITE RELATED Y_2O_3 AND FLUORITE CeO_2 SYSTEMS BASED ON A UNIQUE EFFECTIVE INDEX

T. Mori[1], *T. Ikegami*[1], *H. Yamamura*[2] *and T. Atake*[3]

[1]First Research Group, National Institute for Research in Inorganic Materials, 1-1, Namiki Tsukuba, Ibaraki, 305-0044
[2]Faculty of Engineering, Kanagawa University, 3-27-1, Rokkakubashi, Kanagawa, 221-8686
[3]Materials and Structure Laboratory, Tokyo Institute of Technology, 4259 Nagatsuta-cho Midori-ku, Yokohama, 226-8503 Japan

Abstract

Y_2O_3 has a crystal structure of *c*-type rare-earth oxide. Y_2O_3 does not show an oxide ionic conductivity. On the other hand, CeO_2 based oxide is one of the most interesting of the fluorite oxides since the ionic conductivity of it is higher than that of yttria-stabilized zirconia. However, CeO_2 based oxides are partially reduced and develop electronic conductivity under reduced atmosphere.

In this study, the effective index for the improvement of ionic conductivity in Y_2O_3 and CeO_2 systems was defined using ionic radii from the viewpoint of crystallography. The utility of this effective index on some electrical properties was investigated.

Keywords: ceria, effective index, electrical conductivity, ion transport number of oxygen, yttria

Introduction

Yttria (Y_2O_3) is *c*-type rare-earth oxide. The *c*-type structure of Y_2O_3 is stable up to 1800°C in air [1]. Moreover, this structure has an excellent resistance to hydration [2]. The *c*-type structure is a modified fluorite-type cubic structure with one fourth of the anion sites vacant and regularly arranged. The oxygen vacancy sites that are regularly arranged in the *c*-type structure do not effectively contribute to oxide ion diffusion. Therefore, the mobility of oxide ion in the *c*-type structure is much less than that in the fluorite structure. Y_2O_3 does not show an oxide ionic conductivity [3]. Generally, the oxide ionic conductivity decreases with a large amount of oxygen vacancy more than 5% in the fluorite structure. However, the fluorite type compound δ-Bi_2O_3 that has a large amount of oxygen vacancy such as 25 atomic % in defect fluorite lattice shows high oxide ionic conductivity at the temperature ranging from 700 to 800°C. Accordingly, the increase of disordered oxygen vacancies in *c*-type structure is very important for preparation of high quality electrolyte.

On the other hand, ceria (CeO_2) is a fluorite type material. Di- or trivalent metal oxides such as calcia (CaO) or rare-earth oxide doped CeO_2 possess higher oxide ionic conductivity than YSZ electrolyte [4–6]. At high oxygen partial pressures,

1418–2874/99/ $ 5.00
© 1999 Akadémiai Kiadó, Budapest
Akadémiai Kiadó, Budapest
Kluwer Academic Publishers, Dordrecht

these CeO_2 based oxides show pure oxide ionic conductivity. However, at low oxygen partial pressures, the Ce^{4+} ion can be partially reduced to a Ce^{3+} ion according to the following reaction (1);

$$O_o^x \rightarrow 1/2O_2 + V_o^{\cdot\cdot} + 2e' \quad (1)$$

Quasi-free electrons are introduced into a fluorite lattice in such a reduced atmosphere. Although CeO_2 based oxides exhibit high oxide ionic conductivity in oxidizing atmosphere, such materials are partially reduced and develop electronic conductivity under low oxygen pressures. Stability in both oxidizing and reducing atmosphere is required for oxide ion conductors. Therefore, it is desirable that the CeO_2-based electrolytes would be further improved from the perspective of crystallography.

According to Pauling's first rule, the crystallographic coordination number of the cation is decided by the radius ratio between cation and anion. The crystal structure is dominated by the coordination number of the cation in the case of the oxide [7]. The coordination number of cation in *c*-type structure is six. The ionic radius ratio between cation (r_c) and anion (r_a) shows 0.414 to 0.732 in the case of six fold coordination. On the other hand, the coordination number of cation around anion in fluorite structure is eight. The ionic radius ratio (r_c/r_a) shows 0.732 to 1.0 in the case of eight fold coordination. This radius ratio becomes to 1 when the cation is coordinated by eight anions in none-distorted fluorite crystal structure. The none-distorted fluorite structure would be one of the preferable crystal structures for fast oxide ionic conduction. Therefore, it would be concluded that the ordered oxygen vacancy in *c*-type structure becomes to disordered oxygen vacancy when the radius ratio (r_c/r_a) approaches 1. On one hand, the experimentally observed trends in oxide ionic conductivity within the fluorite type materials have been explained by an ionic radius ratio (r_d/r_h) [8]. In this radius ratio (r_d/r_h), r_d means the ionic radius of dopant, r_h is the ionic radius of the host element. The work of Kilner [8] indicates that the association energy of oxygen vacancies increases with the ionic radius mismatch between dopant cation and the host element. It is inferred that the ionic conductivity in fluorite-related and fluorite oxides could be enhanced by a decrease of this ionic radius mismatch. However, the radius ratio (r_c/r_a) was not fitted to the fluorite-related and fluorite oxides, because this ratio was not reflected in the oxygen defect structure. Moreover, the ionic radius ratio (r_d/r_h) lacked the viewpoint of crystallography. Therefore, high quality electrolytes could not be proposed using these ionic radius ratios.

In this study, a unique effective index is defined in Eq. (2) instead of (r_c/r_a) or (r_d/r_h).

$$\text{Effective index} = (\text{av.}r_c/r_o)\,(r_d/r_h) \quad (2)$$

where av.r_c is the average ionic radius of the cations, r_o is the oxygen ion radius in *c*-type structure (1.40 Å) [9], r_d is the average ionic radius of dopants, r_h is the ionic radius of the host element (Y^{3+} or Ce^{4+}). In the case of CeO_2, the oxygen ion radius of eight-fold coordination is 1.42 Å [9]. The oxygen content in a unite cell of defect

CeO_2 system is (2–δ). δ is the level of oxygen vacancies in the defect CeO_2 system. The existence ratio of oxygen in a unite cell is (2–δ)/2 . In this study, it is assumed that the ion radius of the oxygen in the oxygen vacancy introduced fluorite structure should be adjusted in inverse proportion to the existence ratio of oxygen. Accordingly, the ion radius of oxygen in the defect fluorite structure was calculated by the Eq. (3) as an effective oxygen ion radius.

$$r_o \equiv \text{eff.}r_o = 1.42\{(2\text{-}\delta)/2\} \quad (3)$$

where eff.r_o is effective oxygen ion radius in defect fluorite structure.

The first term in equation [2] becomes 1 when the cation is coordinated by eight anions in the none-distorted fluorite crystal structure [7]. The second term in Eq. (2) approaches 1 when the composition dependence of the ionic conductivity shows a maximum value in the case of the fluorite structure [8]. Therefore, it is assumed that Y_2O_3 and CeO_2 based oxides reach the ideal structure for high oxide ionic conduction when the effective index goes towards 1.

Experimental procedure

Preparation of powder and sintered body

The starting materials for Y_2O_3 system were commercial Y_2O_3 (purity: 99.99%, Nippon yttirum Co. Ltd., Japan), La_2O_3 (purity: >99.95%, Kanto Chemicals Co. Ltd., Japan), CeO_2 (purity: 99.9%, Wako Pure Chemical Industries Ltd., Japan) and $SrCO_3$ (purity: 99.9%, Wako Pure Chemical Industries Ltd., Japan). Each powder was mixed into ethanol by using ball milling for 12 h. The powders were mixed in order to prepare the fixed compositions of $\{La_aSr_{0.025}Ce_{0.25}Y_{(1-a)}\}_2O_3$ (a=0.05, 0.1, and 0.15) and $(Y_{1-x}Ce_x)_2O_3$ (x=0, 0.25 and 0.30). This powder mixture was dried at 100°C for 12 h, and calcined at 1000°C for 1 h. The starting materials used for preparation of CeO_2 based materials were commercial $Ce(NO_3)_3{\cdot}6H_2O$ powder (purity: 99.9%; Kishida Chemical Co. Ltd., Japan), $Sm(NO_3)_3{\cdot}6H_2O$ powder (purity: 99.9%; Kishida Chemical Co. Ltd., Japan), $La(NO_3)_3{\cdot}6H_2O$ powder (purity: 99%; Merck Japan Co. Ltd.), $Ca(NO_3)_2{\cdot}4H_2O$ powder (purity: 99.9%; Kishida Chemical Co. Ltd., Japan) and $Sr(NO_3)_2$ powder (purity: 99%; Kanto Chemical Co. Ltd., Japan). Each powder was dissolved in distilled water, and the solutions were mixed in order to prepare the compositions of $M_xCe_{1-x}O_{2-\delta}$ (M=Sm, La, x=0.125, 0.15, 0.175, 0.2 and 0.25), $(Sm_{0.5}Ca_{0.5})_xCe_{1-x}O_{2-\delta}$ (x=0.175, 0.20, 0.225 and 0.25) and $(La_{1-x}Sr_x)_{0.175}Ce_{0.825}O_{2-\delta}$ (x=0.1, 0.2 and 0.4). NH_3–$(NH_4)_2CO_3$ solution [$NH_3/(NH_4)_2CO_3$ =1/1] was dropped into the mixed solution for precipitation. The powder was dried after filtration and rinsing. The dry powder was calcined at 1000°C for 1 h. These samples were molded under a pressure of 500 kg cm^{-2} and subjected to a rubber press at 2 t cm^{-2} (1 t=10^3 kg) in order to obtain a green body. Sintering conditions were as follows: the sintering temperature of Y_2O_3 based materials and $M_xCe_{1-x}O_{2-\delta}$ (M=Sm, La, x=0.125, 0.15, 0.175, 0.2 and 0.25) was 1550°C and that of the others was 1450°C with a sintering time of 4 h in each case.

Sample characterization and measurement of electrical properties

The sintered samples were fully grounded under 100 mesh, and the crystal phase was identified using XRD (CuK_α, 50 kV, 24 mA). Electrical conductivity of the sintered samples was measured by DC and AC three probe methods at 800°C in air, after a Pt electrode was applied to both sides of the sintered bodies at 1100°C for 1 h in air. The dimensions of the samples were 10 mm diameter and 2 mm thickness. An impedance analyzer (4192A LF, Yokogawa-Hewlett-Packard Ltd., Japan) was used for the AC-conductivity measurements in the frequency range of 10 Hz to 1 MHz. The AC measurements were performed with a sample voltage of 10 mV. A total electrical conductivity (grain boundary plus lattice conductivity) of the samples was depicted as the electrical conductivity. This total conductivity was estimated by using both of the DC-conductivity and the AC-conductivity measurements for confirmation of accuracy in measurement.

The oxygen partial pressure (P_{O_2}) dependence of conductivity in CeO_2 based materials was measured at 800°C. The P_{O_2} was controlled using a zirconia pump from 10^{-3} to 10^{-16} atm and a zirconia oxygen sensor checked it.

The electromotive force (emf_{obs}) of the following gas concentration cell (4) was measured in a mixed flow of O_2 and N_2 at P'_{O_2}=1 atm and P''_{O_2}=0.21 atm by the gas concentration cell method:

$$P'_{O_2}, \text{Pt}|(Y_2O_3 \text{ or } CeO_2 \text{ solid solution})|\text{Pt}, P''_{O_2} \quad (4)$$

The ionic transport number of oxygen, t_i, was estimated as the ratio of the observed *emf* to the theoretical *emf*. The dimensions of the samples were 30 mm square and 2 mm thickness.

Results and discussion

Figure 1 shows the relationship between effective index and electrical conductivity at 800°C. The prepared samples consisted of *c*-type rare earth oxide. No other phases were observed by XRD. The electrical conductivity increased with an increase of the effective index in Fig. 1. In particular, the electrical conductivity of $(La_xSr_{0.025}Ce_{0.25}Y_{0.725-x})_2O_{3.23}$ (x=0.05, 0.1 and 0.15) was higher than that of $(Ce_{0.25}Y_{0.75})_2O_{3.25}$. Although the oxygen vacancy concentration in unite cell was same level comparing with $(Ce_{0.25}Y_{0.75})_2O_{3.25}$. Therefore, it is concluded that this effective index would be useful for introduction of disordered oxygen vacancies in the *c*-type rare earth oxides.

Figure 2 displays the relationship between the effective index and the ionic transport number of oxygen at 800°C. The ionic transport number increased with the increasing of the effective index, confirming utility of the effective index. From the results of Fig. 1 and Fig. 2, it is suggested that the enhancement of electrical conductivity is mainly attributable to the increasing of oxide ionic conductivity. It is concluded that the ordered oxygen vacancies in Y_2O_3 ($(=Y_2(O_{3/4}V_{o1/4})_4)$, $V_o^{\cdot\cdot}$: oxygen vacancy) change to the disordered oxygen vacancies due to the improvement of Y_2O_3 based on the effective index.

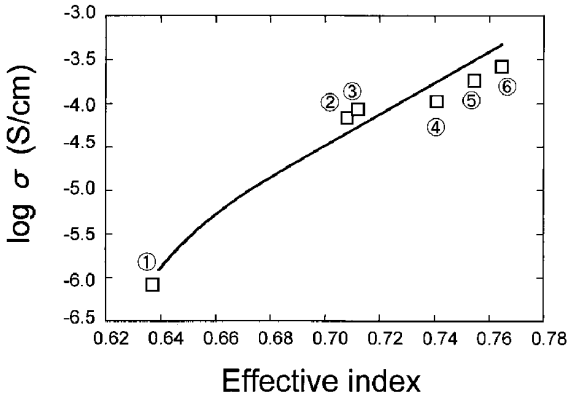

Fig. 1 Relationship between effective index and electrical conductivity of Y_2O_3 based materials. 1 – Y_2O_3 (=$Y_2(O_{3/4}V\ddot{o}_{1/4})_4$), 2 – $(Ce_{0.25}Y_{0.75})_2O_{3.25}$, 3 – $(Ce_{0.3}Y_{0.7})_2O_{3.30}$, 4 – $(La_{0.05}Sr_{0.025}Ce_{0.25}Y_{0.675})_2O_{3.23}$, 5 – $(La_{0.10}Sr_{0.025}Ce_{0.25}Y_{0.625})_2O_{3.23}$, 6 – $(La_{0.15}Sr_{0.025}Ce_{0.25}Y_{0.575})_2O_{3.23}$

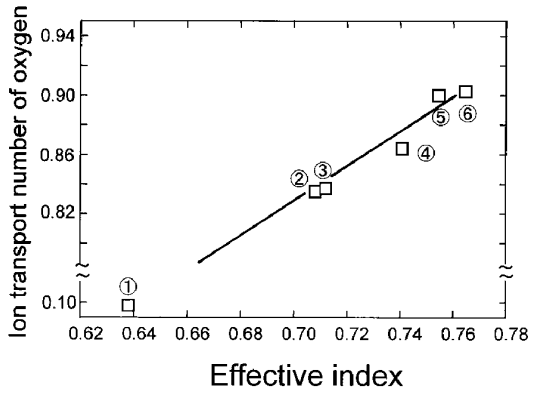

Fig. 2 Relationship between effective index and ion transport number of oxygen of Y_2O_3 based materials. 1 – Y_2O_3 (=$Y_2(O_{3/4}V\ddot{o}_{1/4})_4$), 2 – $(Ce_{0.25}Y_{0.75})_2O_{3.25}$, 3 – $(Ce_{0.3}Y_{0.7})_2O_{3.30}$, 4 – $(La_{0.05}Sr_{0.025}Ce_{0.25}Y_{0.675})_2O_{3.23}$, 5 – $(La_{0.10}Sr_{0.025}Ce_{0.25}Y_{0.625})_2O_{3.23}$, 6 – $(La_{0.15}Sr_{0.025}Ce_{0.25}Y_{0.575})_2O_{3.23}$

Figure 3 shows the relationship between the effective index and the electrical conductivity in CeO_2 based oxides at 800°C. As this figure indicates, the electrical conductivity increased with an increase of this effective index, confirming utility of the index. On the other hand, the electrical conductivity of $(La_{0.6}Sr_{0.4})_{0.175}Ce_{0.825}O_{2-\delta}$ deviated from expectation based on the effective index. It is concluded that the defined index could not apply to the samples including the small level of secondary phase in the grain boundary or associated oxygen vacancy. The ionic transport numbers of oxygen for these samples were almost unity at 800°C. Since the ionic transport number of the specimens remains unity, the enhancement of electrical conductivity in Fig. 3 is attributable to an increase in oxide ionic conductivity.

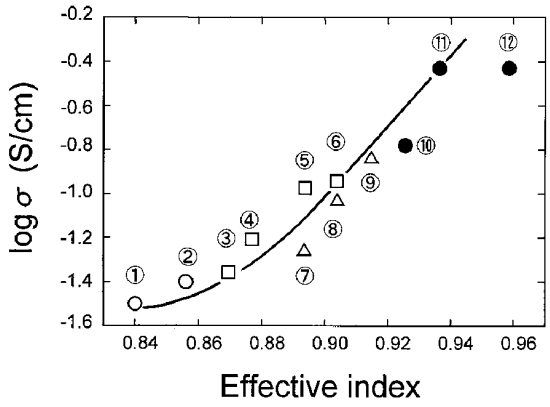

Fig. 3 Relationship between effective index and electrical conductivity of CeO_2 based materials. 1 – $Sm_{0.2}Ce_{0.8}O_{1.9}$, 2 – $Sm_{0.25}Ce_{0.75}O_{1.88}$, 3 – $(Sm_{0.5}Ca_{0.5})_{0.175}Ce_{0.825}O_{1.87}$, 4 – $(Sm_{0.5}Ca_{0.5})_{0.20}Ce_{0.80}O_{1.85}$, 5 – $(Sm_{0.5}Ca_{0.5})_{0.225}Ce_{0.825}O_{1.83}$, 6 – $(Sm_{0.5}Ca_{0.5})_{0.25}Ce_{0.75}O_{1.81}$, 7 – $La_{0.125}Ce_{0.875}O_{1.94}$, 8 – $La_{0.15}Ce_{0.85}O_{1.93}$, 9 – $La_{0.175}Ce_{0.825}O_{1.91}$, 10 – $(La_{0.9}Sr_{0.1})_{0.175}Ce_{0.825}O_{1.90}$, 11 – $(La_{0.8}Sr_{0.2})_{0.175}Ce_{0.825}O_{1.89}$, 12 – $(La_{0.6}Sr_{0.4})_{0.175}Ce_{0.825}O_{1.88}$

The oxygen partial pressure dependence of the ionic conductivity in CeO_2 based oxides at 800°C is shown in Fig. 4. The P_{O_2} dependence of the electrical conductivity obviously consists of two regions. One is the ionic conductive region and the other is the *n*-type semi-conductive region. In the ionic conductive region, the electrical conductivity is constant against P_{O_2}. On the other hand, the electrical conductivity increases in the *n*-type region with decreasing P_{O_2}. The relationship between the logarithm of conductivity and the logarithm of P_{O_2} has a slope of –1/4 [10]. The *n*-type conduction appears because the number of conductive electrons is increased by re-

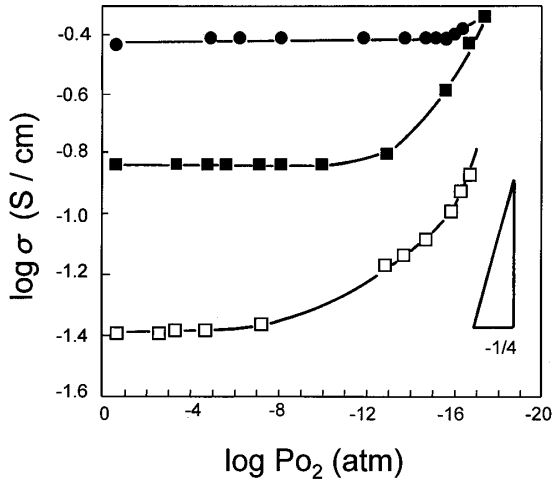

Fig. 4 Oxygen partial pressure dependence of electrical conductivity of CeO_2 based materials. □ – $Sm_{0.25}Ce_{0.75}O_{1.88}$, ■ – $La_{0.175}Ce_{0.825}O_{1.91}$, ● – $(La_{0.8}Sr_{0.2})_{0.175}Ce_{0.825}O_{1.89}$

duction of CeO_2. The oxide ionic conductivity of $Sm_{0.25}Ce_{0.75}O_{1.87}$ and $La_{0.175}Ce_{0.825}O_{1.91}$ was constant up to around $P_{O_2}=10^{-8}$ and 10^{-10} atm, respectively. However, the electrical conductivity increased with decreasing P_{O_2} below $P_{O_2}=10^{-8}$ or 10^{-10} atm due to the reduction of $Sm_{0.25}Ce_{0.75}O_{1.87}$ and $La_{0.175}Ce_{0.825}O_{1.91}$. On the other hand, the electrical conductivity of $(La_{0.8}Sr_{0.2})_{0.175}Ce_{0.825}O_{1.89}$ was constant up to 10^{-16} atm. The ionic conductive regions of $(La_{0.8}Sr_{0.2})_{0.175}Ce_{0.825}O_{1.89}$ continued up to a lower P_{O_2} comparing with the $Sm_{0.25}Ce_{0.75}O_{1.87}$ and $La_{0.175}Ce_{0.825}O_{1.91}$. Therefore, it is found that the reduction resistance of M_2O_3–CeO_2 (*M*=Sm, La) based materials increases with an increase of the effective index. Moreover, the oxide ionic conductivity of $(La_{0.8}Sr_{0.2})_{0.175}Ce_{0.825}O_{1.89}$ having high effective index was higher than the conductivity of $Sm_{0.25}Ce_{0.75}O_{1.87}$ and $La_{0.175}Ce_{0.825}O_{1.91}$. Although the oxygen vacancy concentration in the unite cell was same level comparing with $Sm_{0.25}Ce_{0.75}O_{1.87}$ and $La_{0.175}Ce_{0.825}O_{1.91}$. This result suggested that the disordering of the oxygen vacancy in $(La_{0.8}Sr_{0.2})_{0.175}Ce_{0.825}O_{1.89}$ is more than that of the others. Therefore, it is concluded that the effective index defined in this study would be useful for introduction of disordered oxygen vacancies into the fluorite structure depressing the association and interaction between ions and oxygen vacancies.

Conclusions

The effective index for fast oxide ionic conduction in Y_2O_3 and CeO_2 based oxides were defined using ionic radii and the amount of oxygen vacancy from the viewpoint of crystallography. In the assumption of this study, the crystal structures of Y_2O_3 and CeO_2 based oxide approach the ideal structure for fast oxide ionic conduction when the effective index increases towards 1.

Tetra-, tri- and divalent metal oxides doped Y_2O_3 based materials were prepared based on this unique effective index for enhancement of electrical conductivity. Electrical conductivity of Y_2O_3 based oxides increased with an increase of the effective index. Ionic transport number of oxygen in the samples was also improved by the enhancement of the effective index. Therefore, it is concluded that the effective index was useful for improvement of electrical properties of *c*-type rare earth oxides.

M_2O_3–CeO_2 (*M*=Sm, La) solid solutions were also prepared based on the effective index. The oxide ionic conductivity of the M_2O_3–CeO_2 solid solutions increased with the increasing of effective index. It is found that the electrical conductivity of the M_2O_3–CeO_2 solid solutions was closely related to the effective index. It is confirmed that the enhancement of electrical conductivity for M_2O_3–CeO_2 solid solutions was attributable to the increase of oxide ionic conductivity from the measurement for ionic transport number of oxygen. Moreover, the oxygen partial pressure dependence of conductivity for $Sm_{0.25}Ce_{0.75}O_{1.87}$, $La_{0.175}Ce_{0.825}O_{1.91}$ and $(La_{0.8}Sr_{0.2})_{0.175}Ce_{0.825}O_{1.89}$ was measured at 800°C as typical examples. The oxide ionic conductive regions of $(La_{0.8}Sr_{0.2})_{0.175}Ce_{0.825}O_{1.89}$ continued up to the lower oxygen partial pressures comparing with the others. As a result, it seemed that the oxygen partial pressure dependence of ionic conductivity for CeO_2 based materials was improved by the enhancement of the effective index.

On the other hand, it is well known that the oxide having an excellent oxide ionic conductivity is δ-Bi_2O_3 [11]. This δ-Bi_2O_3 is a polymorph of pure bismuth sesqui-

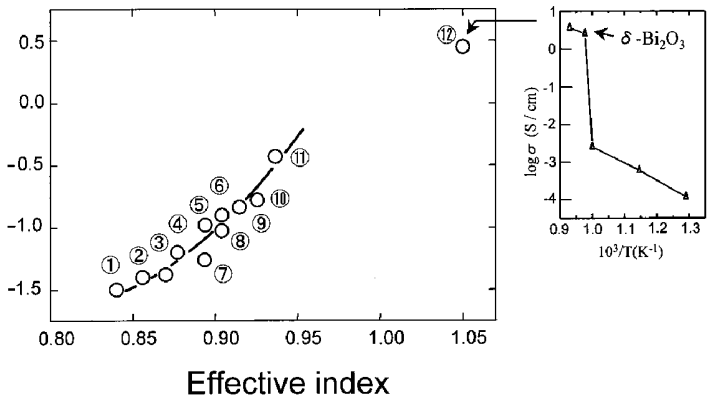

Fig. 5 Relationship between effective index and electrical conductivity of CeO_2 based materials. 1 – $Sm_{0.2}Ce_{0.8}O_{1.9}$, 2 – $Sm_{0.25}Ce_{0.75}O_{1.88}$, 3 – $(Sm_{0.5}Ca_{0.5})_{0.175}Ce_{0.825}O_{1.87}$, 4 – $(Sm_{0.5}Ca_{0.5})_{0.20}Ce_{0.80}O_{1.85}$, 5 – $(Sm_{0.5}Ca_{0.5})_{0.225}Ce_{0.825}O_{1.83}$, 6 – $(Sm_{0.5}Ca_{0.5})_{0.25}Ce_{0.75}O_{1.81}$, 7 – $La_{0.125}Ce_{0.875}O_{1.94}$, 8 – $La_{0.15}Ce_{0.85}O_{1.93}$, 9 – $La_{0.175}Ce_{0.825}O_{1.91}$, 10 – $(La_{0.9}Sr_{0.1})_{0.175}Ce_{0.825}O_{1.90}$, 11 – $(La_{0.8}Sr_{0.2})_{0.175}Ce_{0.825}O_{1.89}$, 12 – δ-$Bi_2O_3$ (=$Bi_4O_6V_{o2}^{\cdot\cdot}$, $V_o^{\cdot\cdot}$: oxygen vacancy, [11])

oxide, this polymorph is stable from 730 to 850°C under oxidation atmosphere. The crystal structure of δ-Bi_2O_3 belongs to defect fluorite-type including a large amount of vacant site in the oxide as expressed as $Bi_4O_6V_{o2}^{\cdot\cdot}$ per unit cell, where $V_o^{\cdot\cdot}$ is the oxygen vacancy [11]. Figure 5 displays the relationship between the effective index and the electrical conductivity at 800°C for the prepared M_2O_3–CeO_2 solid solutions and δ-Bi_2O_3. It is concluded that the result of this figure supported the assumption of this study. The utility of the effective index was confirmed. However, δ-Bi_2O_3 is easily reduced in reducing atmosphere. Accordingly, it is expected that the electrical properties of Y_2O_3 and CeO_2 based materials be improved by the further enhancement of this effective index.

References

1 N. M. Tallan and R. W. Vest, J. Am. Ceram. Soc., 49 (1966) 401.
2 T. Norby and P. Kofstad, J. Am. Ceram. Soc., 69 (1986) 784.
3 R. Gerhardt and A. S. Nowick, J. Am. Ceram. Soc., 69 (1986) 641.
4 D. Singman, J. Electrochem. Soc., 113 (1966) 502.
5 K. Eguchi, T. Kunisaki and H. Arai, J. Am. Ceram. Soc., 69 (1986) C282.
6 D. L. Maricle, T. E. Swarr and S. Karavolis, Solid State Ionics, 52 (1992) 173.
7 Y. M. Chiang, D. Birnie III and W. D. Kingery, 'Physical Ceramics, -Principles for Ceramic Science and Engineering-' John Wiley & Sons, New York 1996, Chapter 1 p. 13.
8 J. A. Kilner, Solid State Ionics, 8 (1983) 201.
9 R. D. Shannon and C. T. Prewitt, Acta Crystallogr., B25 (1969) 925.
10 Y. M. Chiang, D. Birnie III and W. D. Kingery, 'Physical Ceramics, -Principles for Ceramic Science and Engineering-' John Wiley & Sons, New York 1996, Chapter 2 p. 136.
11 T. Takahashi and H. Iwahara, Mat. Res. Bull., 13 (1978) 1447.